

Nernst-Planck transport theory for (reverse) electrodialysis: II. Effect of water transport through ion-exchange membranes

M. Tedesco, H.V.M. Hamelers, and P.M. Biesheuvel*

*Wetsus, European Centre of Excellence for Sustainable Water Technology,
Oostergoweg 9, 8911 MA Leeuwarden, The Netherlands*

Abstract

Transport of water through ion-exchange membranes is of importance both for electrodialysis (ED) and reverse electrodialysis (RED). In this work, we extend our previous theory [J. Membrane Sci., **510**, (2016) 370-381] and include water transport in a two-dimensional model for (R)ED. Following a Maxwell–Stefan (MS) approach, ions in the membrane have friction with the water, pore walls, and one another. We show that when ion-ion friction is neglected, the MS–approach is equivalent to the hydrodynamic theory proposed by Deen for nanofiltration. The model describes all fluxes of ions and water self-consistently as function of the driving forces. After validation against experimental data from literature for ED and RED, the model is also used to analyze single-pass seawater ED and RED with highly concentrated solutions. All fluxes and velocities of water and ions in the membranes are calculated, and the influence of water and coion leakage is investigated under different conditions.

Keywords: Maxwell–Stefan theory, ion-exchange membranes, osmosis, electro-osmosis, hydraulic permeability.

1. Introduction

In electromembrane processes, ion-exchange membranes (IEMs) are used to desalinate water, to selectively remove ions or other charged molecules, and to generate energy from salinity differences [1]. IEMs are membranes that contain fixed charges and allow counterions to pass, while in the ideal case coions and water are completely rejected. For all applications of electromembrane processes, a general membrane transport theory describes ion and water flow as function gradients in electrical potential, salt concentration, and pressure in a self-consistent manner without ad-hoc assumptions.

The complexity of such a general theory depends on the behavior of the membrane: in the ideal case, only counterions pass the membranes, and the mathematical description of membrane transport is the least complex [2]. However, in most cases membranes cannot be described as ideally selective barriers, as they are partially crossed by coions and water, resulting in a decrease of process performance. This non-ideal behavior of membranes requires the simultaneous description of transport of counterions, coions, and water.

* *Corresponding Author* (P. M. Biesheuvel): maarten.biesheuvel@wetsus.nl

The effect of coion transport is often quantified by the permselectivity of membranes, α (or likewise by the counterion transport number, t_{ct}). When measured under standardized conditions, typical values of permselectivity of commercial IEMs are in the range of 96–99% [3]. However, in an actual process these values can be much lower [1, 4].

Water transport through ion-exchange membranes has been addressed both experimentally [5–7] and theoretically [8–10]. Four mechanisms are often considered to cause water transport: I. A hydrostatic pressure difference across the membrane; II. Osmosis, which is water transport due to an osmotic pressure difference across the membrane; III. electro-osmosis, water transport due to ion-water friction; and IV. water transported in the hydration shell around the ions, where water molecules are tightly held. In the present work we focus on mechanisms I–III and neglect mechanism IV. Note that in the present work we use the words “water”, “solvent”, and “fluid” interchangeably.

Although different theoretical approaches have already been proposed, combining ion and water transport in a general model which describes both Electrodialysis (ED) and Reverse Electrodialysis (RED) is still challenging. As an example of such challenges, transport of water is affected by differences across the membrane in salt concentration, electric potential and hydrostatic pressure, as well as by friction with ions and pore walls, and all effects must be included simultaneously [11].

Previously, we developed a two-dimensional electromembrane model based on the approach by Sonin and Probst [2], focusing on the effect of coion transport in ED and RED [1] (See Fig. 1 for a brief description of these processes). Our work showed that in RED coion transport reduces the power density by up to 20%, while for ED the energy consumption increases by at least a factor of three compared to the ideal case [1]. In the present work, we extend the model by including fluid (water) transport through the membranes. We focus on the modeling scale of a single cell pair, because most of the relevant transport phenomena of the (R)ED process relate to the cell level. Stack-level modeling is of importance to identify hydraulic leakage between cells [12], non-uniform flow distribution [13], and parasitic currents in the manifolds [14], but is not discussed. We validate the model against experimental data from literature (both for ED and RED), and use the model to describe quantitatively the effects of coion and water transport.

2. General aspects of ion transport in liquid-filled membrane pores

In (reverse) electrodialysis, transport phenomena in the spacer channel have often been the primary focus of theoretical studies [15–25], with membrane transport described by a constant permselectivity (set to 100%, in many cases) and water flow neglected (with [21] a notable exception). Instead, in the present work we combine a two-dimensional (2D) model for the spacer channels with a detailed description of transport of ions and water through the membranes [26, 27], thus providing a full description of transport phenomena in the channels and in the membranes. In the 2D model, one coordinate axis runs through the cell (from entrance to exit), and one coordinate is directed towards and through the membranes, see Fig. 2. For the modeling of ion electromigration in the spacer channels, we assume that the ions have friction only with the fluid (ion-solvent, or ion-fluid, interaction), while in the membrane we consider that ions also have friction with the membrane matrix

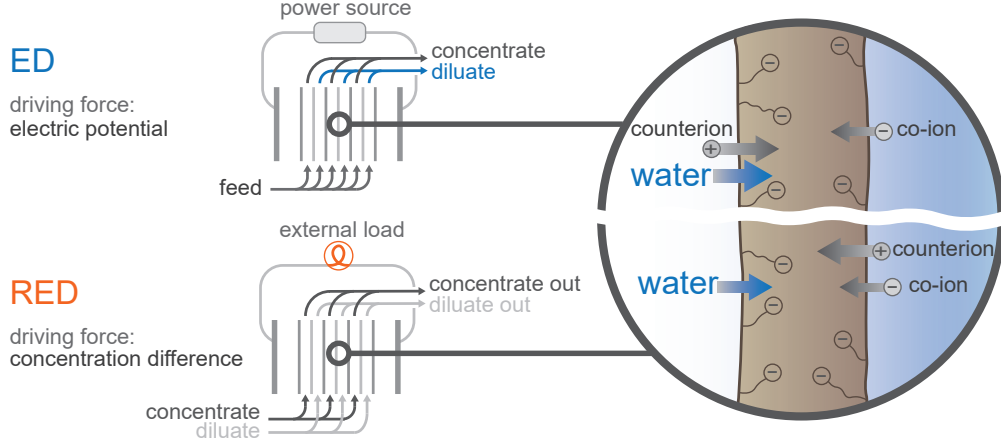


Figure 1: Principle of electrodialysis (ED) and reverse electrodialysis (RED). The ED process is used as a separation process of aqueous streams by applying a voltage across membranes, while RED harvests the concentration difference between two salt solutions for power production. The repeating unit of the system is the cell pair which consists of a concentrate channel, a cation exchange membrane (CEM), a diluate channel, and an anion exchange membrane (AEM).

(‘ion-wall’ or ‘ion-matrix’ interaction), as well as with other ions (‘ion-ion’ interaction), as described by Maxwell-Stefan (MS) theories [26, 28–30].

Following the Maxwell-Stefan framework, the total force acting on an ion i in the membrane can be described as

$$-\nabla \tilde{\mu}_i = R_g T \sum_j f_{i-j} (\mathbf{v}_i - \mathbf{v}_j) \quad (1)$$

where $\tilde{\mu}_i$ is the electrochemical potential of ion i , R_g the gas constant, T temperature, f_{i-j} a friction factor between ion i and phase j (which can be the water, the membrane matrix, or another ion), while \mathbf{v}_i and \mathbf{v}_j are velocities of i and j .

In this work, we assume ideal thermodynamics with ions as point charges and consider the water as a continuum fluid. For ideal thermodynamic behavior of the ions, $\tilde{\mu}_i$ is then equal to

$$\tilde{\mu}_i = \tilde{\mu}_{i,0} + R_g T \ln c_i + RT z_i \phi \quad (2)$$

where c_i is ion concentration, z_i ion valence, ϕ the dimensionless electric potential (which can be multiplied by $V_T = RT/F$ to obtain a dimensional voltage), after which Eq. (1) can be written in a single direction, x , as

$$-\frac{\partial \ln c_i}{\partial x} - z_i \frac{\partial \phi}{\partial x} = \frac{1}{D_{i-F}} (v_i - v_F) + f_{i-m} (v_i - v_m) + \beta c_k (v_i - v_k) \quad (3)$$

where D_{i-F} is an ion-fluid diffusion coefficient, $D_{i-F} = 1/f_{i-F}$, f_{i-m} is a friction factor between ion i and the membrane matrix (which has zero velocity, $v_m = 0$), and v_F is the fluid velocity in the membrane. The last term in Eq. (3) describes friction of ion i with another ion, k , and includes a linear dependence on the concentration of the other ion, and on the velocity difference. Note that in this work concentrations are defined per unit open volume, i.e., per unit aqueous volume in the membrane (or, in spacer channel) [31], while velocities and fluxes are defined per unit total area of a channel or membrane. Neglecting ion-ion friction (setting β to zero), Eq. (3) can be rewritten by

introducing a modified diffusion coefficient, D_i^* , which is defined as

$$\frac{1}{D_i^*} = \frac{1}{D_{i-F}} + f_{i-m} \quad (4)$$

resulting for the ion velocity in the membrane in [32]

$$v_i = \frac{D_i^*}{D_{i-F}} v_F - D_i^* \left(\frac{\partial \ln c_i}{\partial x} + z_i \frac{\partial \phi}{\partial x} \right). \quad (5)$$

Eq. (5) gives the velocity of ion i in an ion-exchange membrane, taking into account ion friction with the fluid and with the membrane matrix. Interestingly, Eq. (5) is formally equivalent to an expression reported by Deen for the filtration of particles through a pore, described by means of two ‘hindrance’ factors, K_c and K_d , where “ c ” and “ d ” refer to “convection” and “diffusion”, respectively [32, 33]. Using Deen’s formalism, Eq. (5) can be rewritten as

$$v_i = K_{c,i} v_F - K_{d,i} D_\infty \left(\frac{\partial \ln c_i}{\partial x} + z_i \frac{\partial \phi}{\partial x} \right) \quad (6)$$

where the equalities $K_{c,i} = D_i^*/D_{i-F}$ and $K_{d,i} = D_i^*/D_\infty$ connect Eqs. (5) and Eq. (6) (where D_∞ is an arbitrary reference value for the diffusion coefficient). The hindrance factors, K_c and K_d , depend on hydrodynamic conditions in the liquid-filled pore, and a number of correlations have been reported to calculate K_c and K_d for the case of neutral (spherical) molecules in cylindrical pores [34, 35].

Using Eq. (6), the ion flux through the membrane, $J_i = c_i v_i$, is now given by [33, 36, 37]

$$J_i = K_{c,i} c_i v_F - K_{d,i} D_{i,\infty} \left(\frac{\partial c_i}{\partial x} + z_i c_i \frac{\partial \phi}{\partial x} \right) \quad (7)$$

which is a general expression for ion transport including ion-fluid and ion-membrane friction. Note that if ion-membrane friction is neglected ($f_{i-m} = 0$), thus $K_{c,i} = 1$ and $K_{d,i} = D_{i-F}/D_{i,\infty}$, Eq. (7) simplifies to

$$J_i = c_i v_F - D_{i,F} \left(\frac{\partial c_i}{\partial x} + z_i c_i \frac{\partial \phi}{\partial x} \right) \quad (8)$$

which is the well-known extended Nernst-Planck (NP) equation [20–23, 38]. Thus, Eq. (7) is a modified NP-equation that includes also ion-wall friction, where K_d and K_c have values between 0 and 1.

The results obtained above demonstrate that, neglecting ion-ion interactions, the Maxwell–Stefan theory gives a framework equivalent to the hydrodynamic theory by Deen for hindered transport of solutes through narrow pores [33]. This equivalence allow us to implement information about solute hindrance into the MS framework. This is advantageous because the hydrodynamic models for solute transport do not include a description of fluid flow, but fluid flow can be included in the MS framework [33]. Note that often calculations using the MS model pre-assign a value to the fluid flow velocity. In contrast, in the present work, all fluxes of solvent and solutes are self-consistently calculated from the balance of driving forces and frictional factors acting on ions and fluid.

3. Model development

Having laid out the general membrane ion transport model, we show how it can be incorporated in a 2D cell model. In the 2D model, ion concentrations in the spacer channel vary in two directions: from membrane to membrane, and from entrance to exit of the cell (along the membrane). A co-

current flow arrangement is considered, where both feed streams flow in the same direction, while the electric field is directed perpendicular to flow, see Fig. 2. We assume steady-state operation, and assume that both in the channel and membranes all diffusive and electromigration fluxes (thus current density) run exactly in the x -direction. We impose constant voltage-conditions, thus the cell pair voltage is the same at each y -coordinate, but the current density changes along y . In the y -direction in the channels, we assume absence of diffusion and electromigration, and the ions are therefore only advected with the fluid. For the fluid, we assume a plug flow profile (y -component of the fluid velocity, v_y , independent of x -coordinate). Because of fluid transport through the membrane, v_y will be y -dependent.

The modeling framework presented here can be used to describe a complete cell pair, i.e., the repeating unit of an (R)ED system. However, to simplify the calculation, we assume in the present work that both the salt molecule and the membranes have “symmetric” properties. In particular, we consider that both AEMs and CEMs have the same physical properties, like porosity, thickness, and magnitude of the membrane charge, and that counterions in the membranes (anions in AEMs, and cations in CEMs) have the same behavior in terms of ion-fluid and ion-membrane friction. The same is assumed to hold for coions. In the spacer channel, we assume that the diffusion coefficient of cation and anion is the same (this assumption is not made for the membrane). Because of these assumptions, the “repeating unit” in the calculation can be reduced to only one membrane, and two “half”-channels (Fig. 2) [1, 2].

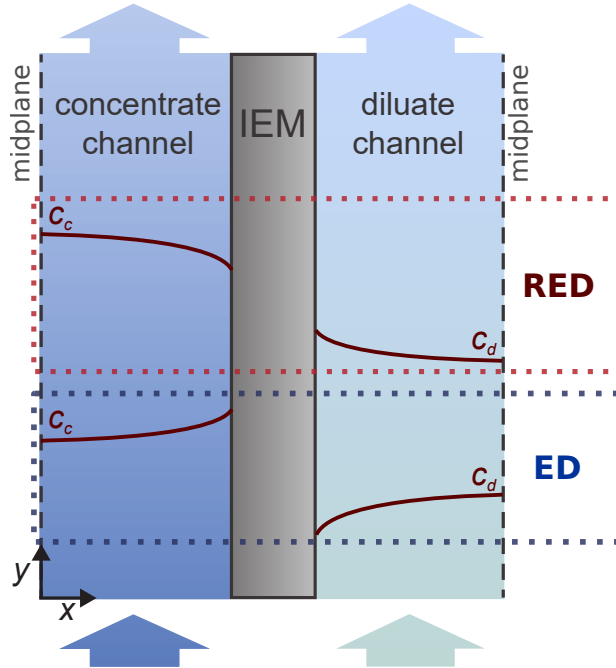


Figure 2: Schematic diagram of the model geometry. The computational domain consists of half of a concentrate channel, one ion exchange membrane (IEM) and half of a dilute channel. Symmetry in x -direction is assumed around the midplanes. Typical concentrations profiles for ED and RED are sketched.

3.1. Modeling the spacer channel

In the 2D model, the ion mass balance in the flow compartment (spacer channel) is given by

$$\epsilon \frac{\partial c_i}{\partial t} + \nabla \cdot J_i = 0 \quad (9)$$

where J_i is the ion flux (defined per total cross-sectional area), and ϵ is the channel porosity (volume left open by spacer mesh). The ion flux, J_i , can be described by the extended Nernst-Planck (NP) equation

$$J_i = c_i \mathbf{v} - D_{i,d} \nabla c_i + D_{i,e} z_i c_i \nabla \phi \quad (10)$$

where \mathbf{v} is the fluid flow velocity in the channel (also defined per total cross-sectional area, i.e., the “empty tube” velocity), and $D_{i,d}$ and $D_{i,e}$ are effective ion diffusion coefficients for diffusion and electromigration. For electromigration, $D_{i,e} = \epsilon / \tau \cdot D_i$ where D_i is the ion diffusion coefficient in free solution, ϵ is the spacer open fraction (porosity) and τ is the tortuosity factor in the channel. For diffusion, the effective coefficient is larger because dispersion effects play a role: because the spacer mesh creates tortuous pathways, the fluid mixes, and thus the concentration is more leveled out. This can be described by adding a dispersion term to the flux equation, which can be combined with the diffusive term and leads to an increase in the coefficient for diffusion (and not for electromigration); thus $D_{i,d} > D_{i,e}$. Substituting Eq. (10) into Eq. (9) leads to

$$\epsilon \frac{\partial c_i}{\partial t} = D_{i,d} \nabla^2 c_i + D_{i,e} z_i \nabla \cdot (c_i \nabla \phi) - \nabla \cdot (c_i \mathbf{v}) \quad (11)$$

which applies to both ions in the spacer channels. In the present work, we consider the system in steady-state, and thus $\partial c_i / \partial t = 0$, while both streams are assumed to contain only a completely dissociated 1:1 salt. We assume that in the spacer channels cations and anions have the same diffusion coefficient ($D_{+,d/e} = D_{-,d/e} = D_{d/e}$), and we neglect diffusion and electromigration in the axial (y -)direction (an assumption discussed in detail in ref. [2]). According to the electroneutrality condition, the concentrations of cation and anion at each point in the spacer channel are equal to each other, thus $c_+ = c_- = c$. Therefore, adding up Eq. (11) for anions and cations results in

$$\frac{\partial}{\partial x} \left(c v_x - D_d \frac{\partial c}{\partial x} \right) + \frac{\partial}{\partial y} (c v_y) = 0 \quad (12)$$

which is the final expression for the salt mass balance for a single 1:1-electrolyte solution. Here the x -coordinate is introduced which runs left to right in Fig. 2, across all three domains. Regarding fluid flow in the channel, a plug flow profile in the y -direction is considered in this work, i.e., v_y is independent of x (though, because of fluid flow through the membrane, v_y will change with coordinate y). Note that for sufficiently thin channels (as for RED), the exact flow profile (parabolic or plug flow) has a negligible effect on the salt flux through the membranes [1]. In order to keep v_y independent of x at all y -positions, the fluid velocity in x -direction, v_x , relates to the fluid velocity in the membrane, v_F , by

$$\frac{\partial v_y}{\partial y} = - \frac{\partial v_x}{\partial x} = \pm \frac{v_F}{h}. \quad (13)$$

where h is the channel half-width and the sign “+” is used for the diluate channel, and “−” for the concentrate channel (following the geometry outlined in Fig. 2). The ionic current density across the

flow channel (in the x -direction) is

$$J_{\text{ch}} = J_+ - J_- \quad (14)$$

where $+$ and $-$ refer to cation and anion. Note that in Eq. (14) J_{ch} is expressed in mol/m²/s, and must be multiplied by F to obtain a current density in A/m², of which the average over the cell will be denoted by I . We define two average salt concentrations, $\langle c \rangle$ and $\langle c \rangle^\dagger$ which are both averages across the width of the channel (in x -direction), and which both depend on y -position. Evaluated at the exit of the cell, one of them, $\langle c \rangle$, is the “mixed cup” effluent concentration. These two concentrations are given by

$$\begin{aligned} \langle c \rangle &= \frac{1}{h} \int_0^h c(x) dx, \\ \frac{1}{\langle c \rangle^\dagger} &= \frac{1}{h} \int_0^h \frac{1}{c(x)} dx. \end{aligned} \quad (15)$$

Combining Eq. (14) with the NP-equation (10), and taking into account that the current density, J_{ch} , is not a function of x (only of y), we can integrate across the width of the flow channel (in x -direction) and arrive at

$$J_{\text{ch}} = -2 \langle c \rangle^\dagger D_e \frac{\Delta\phi}{h} \quad (16)$$

where $\Delta\phi$ is the potential difference across half of the channel.

An overall salt balance over a “slice” with thickness dy in the channel relates the ions flux through the membrane to $\langle c \rangle$ according to

$$J_{\text{ions},m} = J_{+,m} + J_{-,m} = \pm 2h \frac{d(v_y \cdot \langle c \rangle)}{dy}. \quad (17)$$

Interestingly, because of the use of Eqs. (16) and (17), no boundary conditions need to be given at the solution/membrane interface for the gradient in concentration or potential. In the middle of the flow channels, symmetry around the midplane leads to $\partial c / \partial x = 0$.

3.2. Modeling the membrane

In the membrane, local electroneutrality holds at each position,

$$c_+ - c_- + \omega X = 0 \quad (18)$$

where ω is the sign of fixed charge ($\omega = +1$ for AEMs, and $\omega = -1$ for CEMs), and X is the molar concentration of membrane charge, defined per unit volume of solution phase in the membrane [31].

The fluid velocity in the membrane, v_F , can be calculated from [38, 39]

$$\frac{\partial P^t}{\partial x} = f_{F-m} (v_m - v_F) + \sum_i \frac{c_i}{D_{i-F}} (v_i - v_F) \quad (19)$$

with f_{F-m} the fluid-membrane friction factor, and P^t the total pressure, which is hydraulic pressure, P^h , minus osmotic pressure [11, 40, 41]. The total pressure is invariant across the solution/membrane boundary (i.e., across the EDL layer). Note that in Eq. (19) P^t has dimension mol/m³, and can be multiplied by RT to a pressure with unit Pa. In Eq. (19), we assume the ions to be point charges (i.e., without volume), and the summation i runs over all ions. For ions as ideal point charges, the osmotic pressure is equal to the total ion concentration (not salt concentration), multiplied by RT .

Note that Eq. (19) is also valid when the ions have friction with the membrane matrix, and/or with one another. Interestingly, if friction between ions and membrane matrix is neglected (and $v_m = 0$), Eq. (19) simplifies to

$$\frac{\partial P^h}{\partial x} + f_{F-m} v_F = \omega X \frac{\partial \phi}{\partial x} \quad (20)$$

which is the classical result reported by Sonin [40] and Schlögl [42].

Transport of ions in x -direction through the membrane is described by Eq. (3) evaluated separately for the anion and cation, while considering steady-state. Steady state implies that, at a given y -coordinate, the ion flux $J_i = v_i \cdot c_i$ is constant across the membrane, both for anion and cation (also the fluid velocity v_F is constant across the membrane because we neglect the volume of the ions). Instead, ion velocities are not invariant across the membrane (with x -coordinate), as will be shown in the next Section. Using Eqs. (16) and (17), cation and anion fluxes in the membrane, J_+ and J_- , relate to the total ions flux, $J_{\text{ions},m}$, and current density, J_{ch} .

To solve for the ion transport in the membrane, Eq. (3) is developed in two ways: first, it is integrated across the membrane to arrive at an overall expression for ion flux, and second, it is differentiated to arrive at a second order differential equation. In this way, the mathematical code (obtained after numerical discretization) becomes very robust and can easily be solved by any algebraic equation-solver.

The integrated form of Eq. (3) becomes (after multiplying by c_i),

$$-\frac{c_{i,d}^\ominus - c_{i,c}^\ominus}{\delta_m} - \frac{z_i}{\delta_m} \int_0^{\Delta\phi_m} c_i d\phi = \frac{1}{D_{i-F}} (J_i - \langle c_i \rangle v_F) + f_{i-m} J_i + \beta \cdot (\langle c_k \rangle J_i - \langle c_i \rangle J_k) \quad (21)$$

where average concentrations are defined by Eq. (15)a with h replaced by δ_m , and where $c_{i,c/d}^\ominus$ denotes the concentration of ion type i at the membrane/channel interface, but still just in the membrane, at the c or d side. After discretization, the integral involving $d\phi$ can be solved using the trapezoid rule. Differentiating Eq. (3) (multiplied by c_i) leads to

$$\frac{\partial^2 c_i}{\partial x^2} + z_i \frac{\partial}{\partial x} \left(c_i \frac{\partial \phi}{\partial x} \right) = \left(\frac{v_F}{D_{i-F}} + \beta (J_k - J_i) \right) \frac{\partial c_i}{\partial x} \quad (22)$$

where, based on Eq. (18), we made use of $\partial_x c_i = \partial_x c_k$ for a binary 1:1 salt and fixed membrane charge, X . Additionally, for the fluid we use an integrated version of Eq. (19), which leads to

$$-\frac{2}{\delta_m} (c_d^* - c_c^*) = -f_{F-m} v_F + \frac{1}{D_{i-F}} \sum_i \left(J_i - v_F \langle c_i \rangle \right) \quad (23)$$

where $c_{c/d}^*$ is the salt concentration in either the “ c ” or “ d ” channel, right at the membrane/channel interface. In Eq. (23), we assume there is no hydrostatic pressure drop over the membrane. Thus, the pressure decay in y -direction through the spacer channel is the same in each channel, to keep the difference between them (across the membrane) at zero. Interestingly, it is not the case that the hydrostatic pressure is invariant across the inner coordinate of the membrane, and we can calculate its behavior. However, this is not necessary to solve the membrane problem. We do not need to solve a differentiated version of Eq. (19).

Because of the symmetry of our geometry, the flux through one membrane of both ions together, $J_{\text{ions},m}$, equals the salt flux, J_{salt} , transported between the d and c channels. For ED, the ratio of J_{ch} over J_{salt} is the current efficiency, λ , while for RED, the inverse is defined as the salt flux efficiency,

ϑ [1]. Both properties can be analyzed as a local (y -dependent) efficiency, see Fig. 6, but, to compare with data, can also be used as an average over the cell, after first averaging current and salt flux separately (see Eq. (18) in ref. [1], and Fig. 4 for an example).

3.3. Overall and boundary conditions

The cell pair voltage, V_{CP} , is the sum of all voltage differences across a cell pair and can be calculated as

$$V_{CP} = 2 V_T (\Delta\phi_c + \Delta\phi_{D,c} + \Delta\phi_m - \Delta\phi_{D,d} + \Delta\phi_d) \quad (24)$$

where $\Delta\phi_c$, $\Delta\phi_m$ and $\Delta\phi_d$ are the potential drops over the concentrate half-channel, the membrane, and the diluate half-channel, respectively (evaluated as the difference between potential at a position “right” minus “left”); $\Delta\phi_{D,c}$ and $\Delta\phi_{D,d}$ refer to the Donnan potentials arising at the two membrane/channel interfaces; the factor of two is because a cell pair is twice our computational domain.

Though V_{CP} is the same at each y -coordinate, how it splits out in its separate contributions, depends on y -position. The Donnan potentials on each membrane/solution interface, $\Delta\phi_{D,c/d}$ are a function of the membrane charge density, X , and can be calculated as [38, 43, 44]

$$\omega X = 2c_{c/d}^* \sinh(\Delta\phi_{D,c/d}). \quad (25)$$

The concentration of an ion i just in the membrane, c_i^\ominus , relates to that just outside according to Boltzmann’s law, $c_{c/d,i}^\ominus = c_{c/d}^* \exp(-z_i \Delta\phi_{D,c/d})$.

This set of equations describes ion and water flow in a 2D model for the (R)ED cell and can be solved for any set of input conditions (flow rates, inlet salt concentrations, cell pair voltage V_{CP} or average current I), together with values for ion diffusion coefficients, ion-membrane frictions, the fluid-membrane friction (water permeability), and membrane thickness and charge, δ_m and X . The differential equations are discretized in x - and y -direction, and the resulting set of algebraic equations solved. Like in ref. [1], discretization in the y -direction is by the implicit (backward) Euler method, and in the x -direction we use a central difference method. Note that the cell pair voltage V_{CP} is constant along the y -coordinate, as is expected for (R)ED cells with unsegmented electrodes. However, fluxes in x -direction (current, ion flux, fluid flow) vary with y -coordinate. Average current density, water velocity and salt flux, as presented in Figs. 3 and 7, are values averaged from entrance to exit of the cell (over the entire y -coordinate).

4. Results and discussion

In the next section we show results of validation of our model against experimental data for RED and ED, as well as additional model calculations for RED at higher salt concentration, and for single-pass seawater desalination by ED. We address the influence of water and coion transport on process performance.

4.1. Model validation for Reverse Electrodialysis

To validate the model, in which all fluxes through the membrane, including fluid flow, are self-consistently calculated from the applied driving forces (which all change between entrance and exit

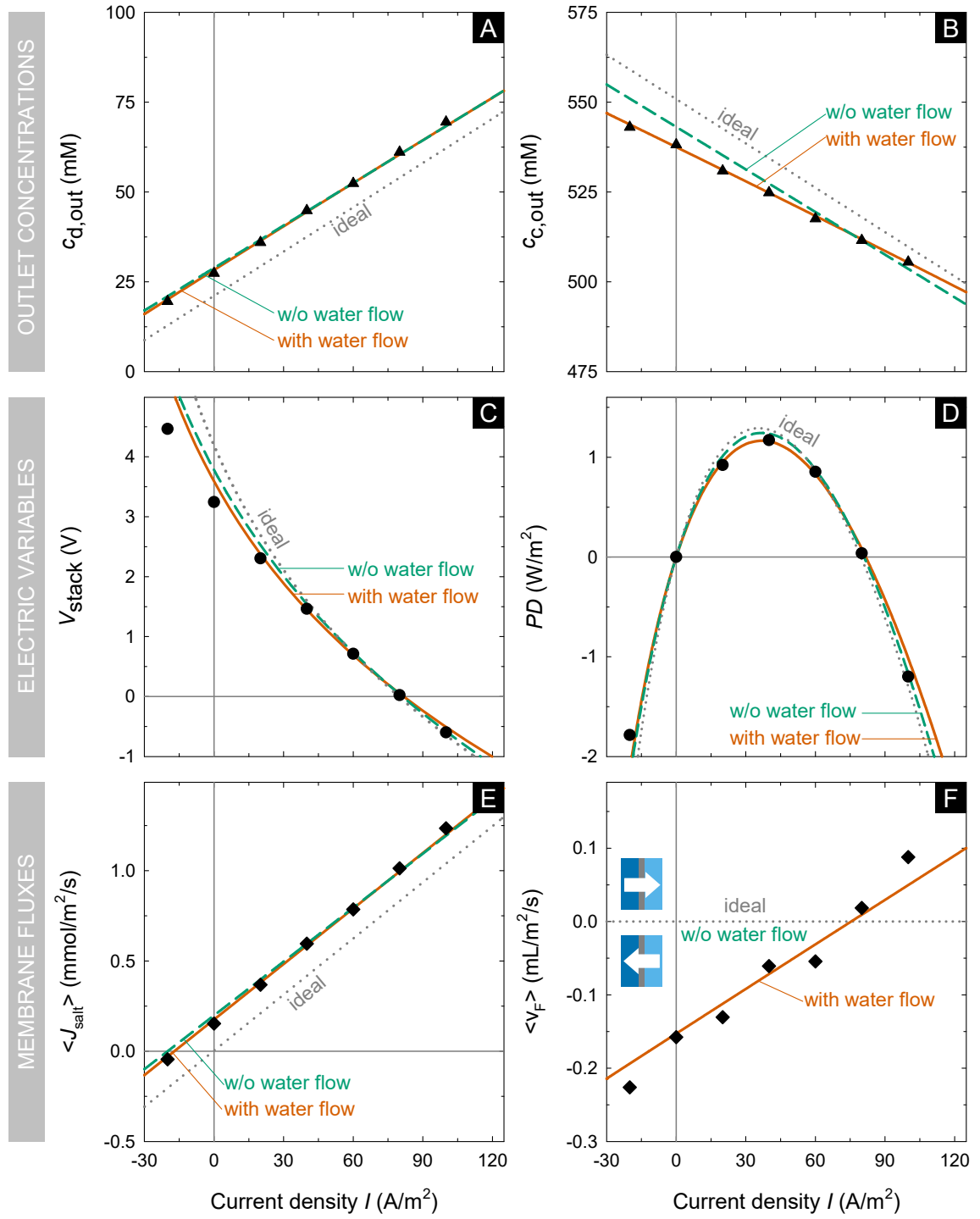


Figure 3: Model validation for an RED stack with 25 cell pairs by comparison with data (symbols) of Veerman *et al.* [45] as function of average current density. A,B) River water and seawater outlet concentration, $c_{d,out}$, $c_{c,out}$. C) Stack voltage, V_{stack} . D) Power density, PD , per m^2 of total membrane area (both AEMs and CEMs combined). E) Average salt flux, $\langle J_{salt} \rangle$. F) Average membrane fluid velocity, $\langle v_F \rangle$. Lines are model predictions, where solid lines include coion and water transport; dashed lines: with coion transport, no water transport; dotted lines: no coion transport and no water transport, i.e., ideal membranes. The region with $\langle J_{ch} \rangle > 0$ and $V_{stack} > 0$ refers to RED-mode; $\langle J_{salt} \rangle < 0$: ED-mode; the region with $V_{stack} < 0$ is ‘forced RED’, or ‘assisted RED’.

of the cell), calculation results are first of all compared with a representative data set for RED from Veerman *et al.* [45]. After having obtained a good fit of the model to the data, to single out the effect of water and coion transport on output parameters, we will reduce the complexity of the full model in a step-wise fashion, and report on three different cases: (1) the full model, which considers the fluxes of counterions, coions and water through the membrane; (2) a model where the flux of water (fluid flow) is set to zero; (3) a further simplified model, in which both the water flux and coion transport are set to zero, and coions are excluded from the membrane, thus simulating the case of ideal (100% permselective) membranes.

The experiments by Veerman *et al.* [45] were done in a stack consisting of 25 cell pairs, contains Sefar Nitex spacers with a thickness of $\delta_{sp} = 200 \mu\text{m}$ and Fumasep FAD/FKD membranes with a thickness $\delta_m = 80 \mu\text{m}$ and membrane charge of $X \sim 4.0 \text{ M}$ [46]. Inlet salt concentrations are 21 and 551 mM of NaCl, for river and seawater. The membrane area is $10 \times 10 \text{ cm}^2$ and the feed flow rate per channel 15.12 mL/min (without water flow through the membranes, the “empty tube” residence time is 7.94 s).

For the membrane, the model has a total of six mobility factors, being the diffusion coefficients of counterion (ct) and coion (co) in the membrane (D_{ct-F} , D_{co-F}), the friction factor between counter- and coions, β , the friction of ions with the membrane matrix (f_{ct-m} , f_{co-m}), and the water-membrane friction (related to hydraulic permeability), f_{F-m} . Furthermore, as free parameters we have the membrane charge density X and, for the spacer channel, the values of D_d and D_e (assumed the same for both ions). The model validation is performed by fitting five experimental conditions: two values of the effluent concentration for the diluate (at two different stack voltages), and two times for the concentrated solution, as well as the current at short-circuit (when $V_{stack} = 0$). With these five constraints, the optimal parameters to fit the theory to the data are found using a Nelder-Mead method.

In preliminary calculations, we found that ion-wall friction in the membrane did not play an important role, and thus the results reported in this work are based on the assumption that the ion-wall friction is zero. Therefore, in the model ions have friction with the fluid, and with other ions. For the ion-fluid diffusion coefficients, the optimal values found are $D_{ct-F} = 78 \mu\text{m}^2/\text{s}$ and $D_{co-F} = 162 \mu\text{m}^2/\text{s}$, which are respectively $\sim 5\%$ and $\sim 10\%$ of the diffusion coefficient at infinite dilution, D_∞ (where $D_\infty = \sqrt{D_{\infty,Na^+} D_{\infty,Cl^-}} = 1640 \mu\text{m}^2/\text{s}$). Thus, for the counterion, the diffusion coefficient is reduced by a factor of ~ 20 , and for the coion by a factor of 10. Furthermore, we find the best fit using a membrane charge density of $X = 4.2 \text{ M}$, an ion-ion friction of $\beta \sim 0.60 \text{ s}\cdot\text{m}/\mu\text{mol}$, a water-membrane friction of $f_{F-m} = 18 \text{ Tmol}\cdot\text{s}/\text{m}^5$ (corresponding to a water permeability of $L_p = 100 \text{ mL}/\text{m}^2/\text{bar}/\text{hr}$).

For the spacer channel, optimal values are $D_d = 1640 \mu\text{m}^2/\text{s}$ and $D_e = 515 \mu\text{m}^2/\text{s}$, where D_d is larger than D_e because it includes dispersion (which enhances concentration equalization). The ratio D_e/D_∞ can be ascribed to a reduction in effective diffusion coefficient due to the spacer porosity ϵ and tortuosity factor τ [47]. In this case, we obtain for the spacer channel a value of $\epsilon/\tau \sim 0.314$. All of these values are very realistic, with the diffusion coefficients of the ion in the membrane, D_{i-F}

about 5-10% of the value in free solution, as reported earlier [48]. Membrane charge density is close to the value reported by Güler *et al.* [46]. The value for the water-membrane friction, f_{F-m} , will be discussed further on.

Fig. 3 shows a comparison between model predictions and experimental data for the outlet salt concentrations, $c_{c,out}$, $c_{d,out}$, stack voltage, V_{stack} , power density, PD , average salt flux, $\langle J_{salt} \rangle$, and fluid velocity through the membrane, $\langle v_F \rangle$. Model predictions agree well with data, not only in the RED regime, but also for the data in ED mode (where $\langle J_{salt} \rangle < 0$), and in the ‘forced RED’ regime ($V_{stack} < 0$). Moreover, the model reproduces the non-linear dependence of voltage on current (Fig. 3C) due to the change in internal resistance because of ion transport.

4.2. Evaluation of ion and water velocities in RED

Based on the model results, it is interesting to analyze the details of membrane transport at the condition of maximum power production, i.e., at a current of 40 A/m², at a position half-way along the channel. Model calculations show that, across the membrane, the concentration of each ion decays quite linearly from the concentrate-side to the diluate-side, with a gradient of about 0.8 mM/ μ m. The electric potential also changes gradually, with a mere 5 mV drop across the membrane. The fluid velocity is about $v_F = -0.075 \mu\text{m/s}$ (see Fig. 3.F), directed towards the concentrate side.

Both ions move in the other direction, towards the diluate side, with the counterion having a velocity of $v_{ct} \sim 0.12 \mu\text{m/s}$. This velocity is almost independent of x -position in the membrane because the counterion concentration is quite constant across the membrane, and only slightly changes from ~ 4.27 M to ~ 4.20 M. However, for the coion the situation is totally different: it diffuses faster and its velocity is not constant. At the concentrate side, the coion has a velocity of $v_{co} = 1.3 \mu\text{m/s}$, and near the diluate side it accelerates in the very last few percent of the membrane to a velocity almost 200 times higher. We do not know whether forces associated with this strong acceleration of the coion need to be considered in the transport theory, nor would we know how to do so. This coion acceleration is related to the linear decay of coion concentration, from around 65 mM on the concentrate-side, to ~ 0.4 mM on the diluate side. This reduction in concentration, at constant ion flux (steady state), must lead to an increase in ion velocity that is inversely proportional to concentration.

Despite its low average concentration, it is due to its high velocity ($\sim 2.5 \mu\text{m/s}$ in the middle of the membrane), that the coion nevertheless has a quite significant flux ($\sim 18\%$ of that of the counterion), i.e., the salt flux efficiency $\vartheta = J_{ch}/J_{salt}$ is only 70 % [1].

It is of interest to understand the origin of the high flux of the coions. Focusing on a position half-way in the membrane, here the counterion concentration is 4234 mM and the coion concentration 34 mM ($125\times$ less than counterions). Three effect jointly explain the high coion flux (a fourth effect reduces the coion flux). I). The total force acting on an anion is around 9 times higher than for counterions. This can be explained as follows. The diffusional force on an ion scales with $F_d = -\ln c/dx = -1/c \cdot dc/dx$ and while the gradient $-dc/dx$ is the same for counter- and coion, the prefactor $1/c$ is $125\times$ higher for the coion, thus making the diffusional force higher for the coion by that factor. However, for counterions the electric field is an additional driving force which is about $11\times$

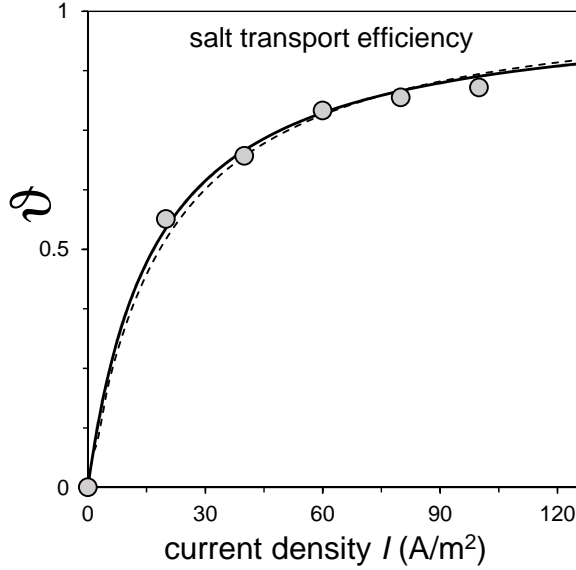


Figure 4: Data and theory for the cell-average salt transport efficiency in reverse electrodialysis, ϑ , as function of cell-average current I , in line with results in Fig. 3.

larger. For coions, the electric field is in magnitude equally large, but relatively to diffusion, not $11\times$ larger (as for counterions), but $11\times$ smaller. II). Both ions move against the direction of fluid, which reduces their flux. While this effect is small for the coion (it goes between 20 and $2000\times$ faster than the fluid), it is significant for the counterion, whose velocity relative to the membrane is around 60% of its velocity relative to the fluid. III). Finally, the coion has a diffusion coefficient that is $2.1\times$ that of the counterion. IV). Whereas ion-ion friction hardly influences the counterion force balance, it consumes 25% of the force on coions (coions are retarded because of ion-ion friction with the much slower counterions). Combining these effects, we find that the coion flux is $\sim 9/125/0.6 \cdot 2.1 \cdot 0.75 = 18\%$ of the counterion flux.

The use of a higher fixed charge density in the membranes (increasing X from 4.2 M as considered above, to a very high value of $X = 6$ M), helps to reduce coion leakage and increases ϑ , but not dramatically. With $X = 6$ M membrane charge, the coion concentration at the high concentration-side decreases from about 65 mM to 45 mM, the coion flux drops by some 35% , and ϑ increases from 70% to 79% . These results show that for RED, in actual operation the permselectivity (or, transport number) is not close to 100% , as suggested by standard membrane characterization methods, but instead, in practice is significantly lower [1]. Fig. 4 shows the excellent fit of theory to data for ϑ based on the results in Fig. 3.

With the full model (that includes water flow and transport of both ions) successfully fitted to the data, it is now interesting to reduce the model complexity by first setting the water flow velocity to zero, and next also to exclude coion flow, and compare the three calculations. First, we set the water velocity through the membrane, v_F , to zero in the model, to arrive at the dashed lines in Fig. 3. Without water flow, the two channels will have the same inflow as outflow volume flux, and thus the two lines for effluent concentration in Fig. 3.A–B must become anti-parallel, i.e., their summation

must be constant, equal to the sum of the two inlet concentrations. Notably, a significant change of $c_{c,out}$ is predicted in this case (Fig. 3.B), and this difference is due to the effect of water flow through the membrane. The salt flux (Fig. 3.E) is hardly changed, thus also ϑ is almost the same. At the condition of maximum power density, the current is slightly higher, as well as the power density (+7%).

If coions are now also excluded from the membrane, power density further increases (another +4 % compared to the “no water flow”-case) and Fig. 3.C shows that the cell voltage at zero current (i.e., the open circuit voltage, OCV) predicted by the full model is significantly lower than in the ideal case ($V_{stack} = 3.6$ vs. 4.2 V). This ratio of OCVs can be directly related to the “apparent” permselectivity of the membranes, α , which can be calculated as the ratio of the OCV-values in the ideal and non-ideal case [49]. In particular, from Fig. 3.C a value of $\alpha = 86$ % is obtained, lower than the nominal values of α beyond 95 % based on a membrane characterization test for Fumatech FAD/FKD membranes [1]. The ratio of salt flux over current density, ϑ , is about $\sim 70\%$ at maximum power, see Fig. 4.

The results above demonstrate that the model can predict performance of an RED process in a wide range of applied currents, and that to describe data accurately, water flow is ideally included. Water flow reduces the power density (7% at maximum power; and an additional 4% because of coion leakage), and the water flow velocity v_F in the membrane is not small: it is of the same order of magnitude as the counterion velocity, and has an effect on the predicted profiles for effluent concentration.

The procedure to fit the theory to the data resulted in a value for the water permeability of $f_{F-m} = 18$ Tmol·s/m⁵. This number can be multiplied by the membrane thickness, δ_m and by $R_g T \sim 2500$ J/mol, and then inverted, to give a water permeability of $L_p = 100$ mL/m²/hr/bar. This is almost 20x higher than what is reported in literature for commercial IEMs [3]. At the end of this section we derive an effective pore size based on this value of L_p .

4.3. Effect of water transport in RED with highly concentrated brines

In this sub-section we analyze the importance of water flow and coion leakage for RED at a higher starting concentration of the concentrate stream (brine), up to 2.0 M, which can be advantageous for energy production (when these highly concentrated brines are available) [50]. Results are presented in Fig. 5, where all parameter settings are the same as in the previous section, including river water concentration (21 mM), except for the brine concentration.

Instead of presenting full curves for stack voltage and power density versus current density, as in Fig.3C,D, here we determine for each such curve the point where the response product (RP) [45] of power \times efficiency is at a maximum. Efficiency and power at that point are presented in Fig. 5. Efficiency is defined as the electric power extracted over the loss of Gibbs energy (which is based on calculation of $2R_g T \phi c \ln c$ over all inlet and outlet streams, and taking the difference, where ϕ is the flow rate). Fig. 5 shows that with increasing brine concentration, the power that can be extracted (at the point of maximum RP) increases, but efficiency goes down. For ideal membranes the efficiency

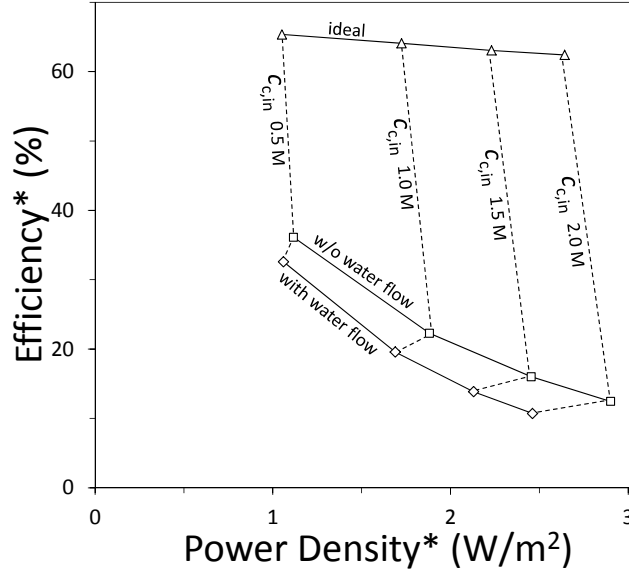


Figure 5: Effect of inlet brine concentration, $c_{c,in}$, on the performance of the RED process. Efficiency is plotted versus power density, for conditions where the response product of efficiency times power is at a maximum.

is by far the highest, even though power (at the point of maximum RP) is similar to the cases with coion transport and with/without water flow. Comparing these two “non-ideal” cases, without water flow both efficiency and power density are higher than with water flow.

Thus, for all salt concentrations, both coion and water transport play an important role, either bringing down process efficiency, power density, or both. The exact analysis of these energy losses due to water and coion transport are of particular relevance for processes in which feed solutions are used in a closed loop circuit, for example in energy storage systems [51, 52].

4.4. Effect of water transport in single-pass ED for seawater desalination

In this section, we analyze steady-state single-pass ED experiments to obtain fresh water from seawater, both with and without water flow through the membrane, see Fig. 6. We look into detail into the velocities of ions in the membrane, including all driving forces. The system is modeled using the same geometry and parameter settings obtained for the RED-calculations in the previous section. We first consider the situation that the concentration difference across the membrane is still small, at the same 40 A/m^2 current as analyzed in detail for RED. In this case, counterions move to the concentrate-side with a velocity of $0.1 \mu\text{m/s}$, while water flows in the same direction, only by drag of the counterions (electro-osmosis), at a velocity of $\sim 0.7 \mu\text{m/s}$.

Since the water flows only because it is dragged by the ions (which are mainly counterions in the membrane) (there is no osmotic pressure difference across the membrane in this calculation), counterions must be faster than the water. Calculations show that this is indeed the case, although the velocity difference is small. In this calculation, the only driving force for ions is the electric potential difference, which is just 0.63 mV across the membrane. Interestingly, the coion has a velocity relative to the water towards the diluate side, but relative to the membrane it moves towards the concentrate side, with a velocity about 2x less than the counterion. This means that according

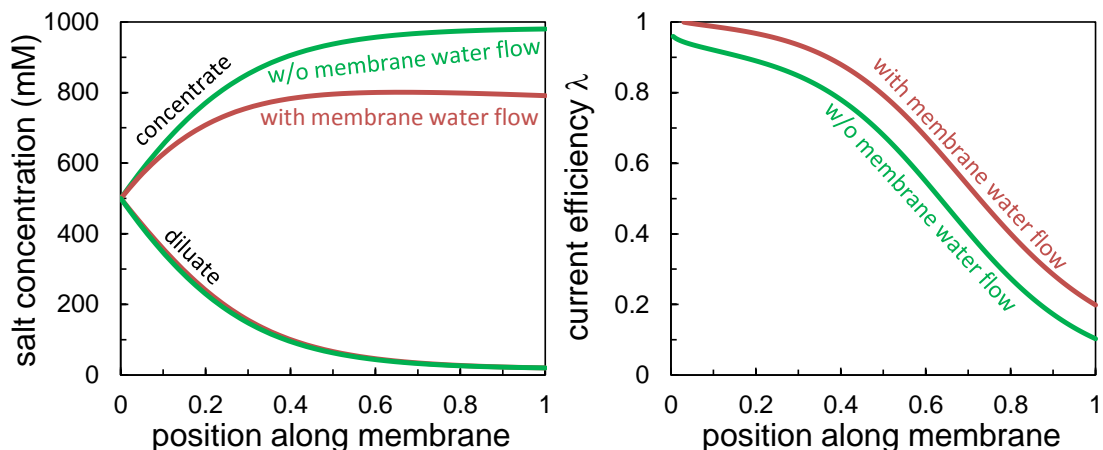


Figure 6: Effect of membrane water transport on single pass seawater ED (to 20 mM in diluate channel). A) Profile of average salt concentration as function of position y . B) Local current efficiency λ .

to the calculation, current efficiency λ is slightly larger than unity (1.01). For the counterion, the main frictional force is due to ion-water friction, but for the coion, ion-ion friction is about equally important as ion-water friction.

This situation changes dramatically when we consider a situation of seawater desalination to freshwater at 20 mM. The (“empty tube”) residence time is set to 30 s (8 s in the previous RED-calculations), and the average current is $\sim 340 \text{ A/m}^2$ ($V_{CP} \sim 0.30 \text{ V}$), in order to reach a diluate concentration of 20 mM at the outlet of the cell. Because of the long residence time, and high current, water flow through the membrane is significant, such that the effluent flow rate in the diluate channel is only 75 % of the inlet value. Analyzing exactly half-way in the cell, where the concentrate has an average concentration of 795 mM and the freshwater of 66 mM, we have a situation that in the membrane the counterion has a net velocity to the concentrate-side of $\sim 0.42 \mu\text{m/s}$, but is outrun by the water, which flows at a velocity of $\sim 0.56 \mu\text{m/s}$. Apparently, the concentration difference created earlier in the cell now pulls water through the membrane, in this way diluting the concentrate. At the same time, the coion moves to the freshwater side at a velocity which changes across the membrane from $1.1 \mu\text{m/s}$ on the concentrate side, to a value several hundred times higher on the diluate side. At this position, half-way in the cell, current efficiency λ is 83 %. Driving forces on the counterion (which relative to the water is moving to the freshwater side) are both diffusion and migration while for the coion it is only diffusion.

Without water flow, to reach 20 mM in the freshwater channel (with the same 30 s residence time), the average current must be higher, $\sim 380 \text{ A/m}^2$ ($V_{CP} \sim 0.41 \text{ V}$). Considering now a point halfway in the channel but for otherwise the same conditions, the counterion velocity is slightly higher, at $\sim 0.51 \mu\text{m/s}$ (towards the concentrate side), the water velocity is zero, and the coion has a velocity (towards the diluate side) that changes from $\sim 1.8 \mu\text{m/s}$ at the concentrate-side to a number 500x higher on the other side, close to 1 mm/s. Because the counterion cannot profit from the water flowing in the same direction, a much higher voltage drop across the (inner coordinate) of the membrane is needed, from 2.4 mV with water flow, to 15 mV in the case without water flow. Counterions move to the

concentrate-side, driven by migration, while migration and diffusion both aid the coion to flow to the diluate side. Current efficiency is only $\lambda = 71 \%$.

With or without water flow, for the counterions only friction with the fluid is of significance (ion-ion friction perhaps 5% relative to ion-fluid friction). However, for the coion, ion-ion friction is much more significant, up to 40 % of the ion-fluid friction with water flow, and up to 50 % without water flow. These calculations show that water transport has myriad effects on operation of an ED cell with high single-pass desalination. Further on we discuss results of a more common batch-wise seawater ED operation and compare with data. For the calculations just made we are not aware of suitable data for comparison and model validation. Especially of importance is the value of hydraulic permeability, L_p , and the question whether a lower value is not more realistic for commercial membranes. The calculations above show the dire consequences that water transfer can have, including a large dilution of the diluate compartment.

Returning one last time to Fig. 6, one unexpected observation is the effect of water flow on energy consumption (current times voltage), and we observed that without water flow, the electric energy input is 50% higher in the cell. When calculated per m^3 of freshwater produced the difference is less, but still $\sim 14 \%$ higher. This might suggest that an ED process with water flow through the membrane makes desalination more energy-efficient, which seems counterintuitive. However, note that with water flow through the membrane the water recovery is reduced to 38 % (from 50 % without water flow). Desalination is less energy consuming at a lower water recovery and this explains why ED with membrane water flow seems to be more energy efficient. In a further calculation for the case with water flow, we increased the diluate flowrate (and reduced the concentrate flowrate) to reach a water recovery of 50% with a 20 mM final concentration. In this last case, the energy consumption is higher than the case without membrane water flow by 12 % ($I \sim 453 \text{ A/m}^2$, $V_{CP} \sim 0.38 \text{ V}$, 66 % of total inflow directed to diluate channel). Thus, according to this calculation, as long as the desalination objective function is correctly defined, water flow through membranes increases energy consumption.

4.5. Effect of water transport in batch-mode ED for seawater desalination

The model calculations just discussed are for single pass seawater ED, for which no data are yet available. In a different experiment, seawater is desalinated in batch mode. Here the initial salt concentration in a diluate and a concentrate reservoir (“bulk” in Fig. 7) is $c_{ini} \sim 510 \text{ mM}$, and the effluent of the ED stack is returned to the reservoirs. The system is run at a constant current density, in the range of $J_{ch} = 10\text{--}200 \text{ A/m}^2$. We make calculations with the same test conditions as reported by Galama *et al.* [53]. The ED system consists of a 10-cell pair stack (membrane area $10 \times 10 \text{ cm}^2$), equipped with Neosepta ACS/CMS membranes (Tokuyama Co., Japan; $\delta_m = 130 \text{ }\mu\text{m}$) and $\delta_{sp} = 500 \text{ }\mu\text{m}$ spacers (Sefar Nitex 06-700/53). The stack is fed in batch mode from two 1 L reservoirs, with a constant feed flow rate of $Q_{in} = 150 \text{ mL/min}$ (i.e., an inflow fluid velocity in the channel $v_{inflow} = 0.5 \text{ cm/s}$). The membrane thickness is $\delta_m = 130 \text{ }\mu\text{m}$, and $X \sim 5.0 \text{ M}$. Theory includes an overall reservoir balance for volume and for total salt. For the ED stack, because of the low desalination per pass, we

discretize using only one grid point in y -direction (i.e., conditions in the cell equal exit conditions).

Results of the fit of the model to the data are shown in Fig. 7, for the reservoir concentrations $c_{c,bulk}$, $c_{d,bulk}$, cell pair voltage, V_{CP} , energy consumption, EC , salt flux, J_{salt} , and fluid velocity through the membrane, v_F . The final panels show the decrease in volume in the diluate reservoir, and the current efficiency (ratio of salt flux over current), where the solid lines are based on theory and the dashed line is a fit through the data. A very good fit to the full data set can be obtained, though interestingly, according to the theory the current efficiency λ decreases in time, while the data show that the current efficiency is rather constant, at around 95 %.

The fit of theory to data results in the following parameter settings: $D_{ct-F} = 50 \mu\text{m}^2/\text{s}$, $D_{co-F} = 75 \mu\text{m}^2/\text{s}$, $X = 5.28 \text{ M}$, $D_d = 525 \mu\text{m}^2/\text{s}$, $D_e = 178 \mu\text{m}^2/\text{s}$, $\beta = 0.60 \text{ s}\cdot\text{m}/\mu\text{mol}$ and $L_p = 4.7 \text{ mL}/\text{m}^2/\text{bar}/\text{hr}$ ($f_{F-m} = 234 \text{ Tmol}\cdot\text{s}/\text{m}^5$). Interestingly, water permeability L_p is now in line with values of commercial membranes [3], unlike the value of L_p used to fit the RED-experiments. The values of the diffusion and electromigration coefficients in the channel, D_d and D_e , are about 3x lower than in the RED-experiments. In the membrane, D_{co-F} and D_{ct-F} are slightly lower than for the RED-experiment, and again we find $D_{co-F} > D_{ct-F}$. The ion-ion friction in the membrane, β , is the same as before. The fitted value for X is higher than for the RED-experiments, and is in line with the higher X reported for Neosepta membranes relative to Fumasep membranes.

Finally, we use the Hagen-Poiseuille equation for cylindrical straight pores and calculate the equivalent pore size d_{eq} for the derived value of L_p . We assume a membrane porosity ϵ_m of 30 %. Using $d_{eq}^2 = 32 \cdot L_{p,exp} \cdot \delta_m \cdot \mu_w / \epsilon_m$ where μ_w is the dynamic viscosity of water ($\sim 1 \text{ mPa}\cdot\text{s}$), we arrive for the two membranes at an equivalent diameter of $d_{eq} \sim 1.5 \text{ nm}$ (RED-experiment) and 0.43 nm (ED-experiment). These are very realistic numbers for the pore size of (R)ED membranes, considering also that due to pore tortuosity (not included in this calculation) the actual pore size is larger than d_{eq} .

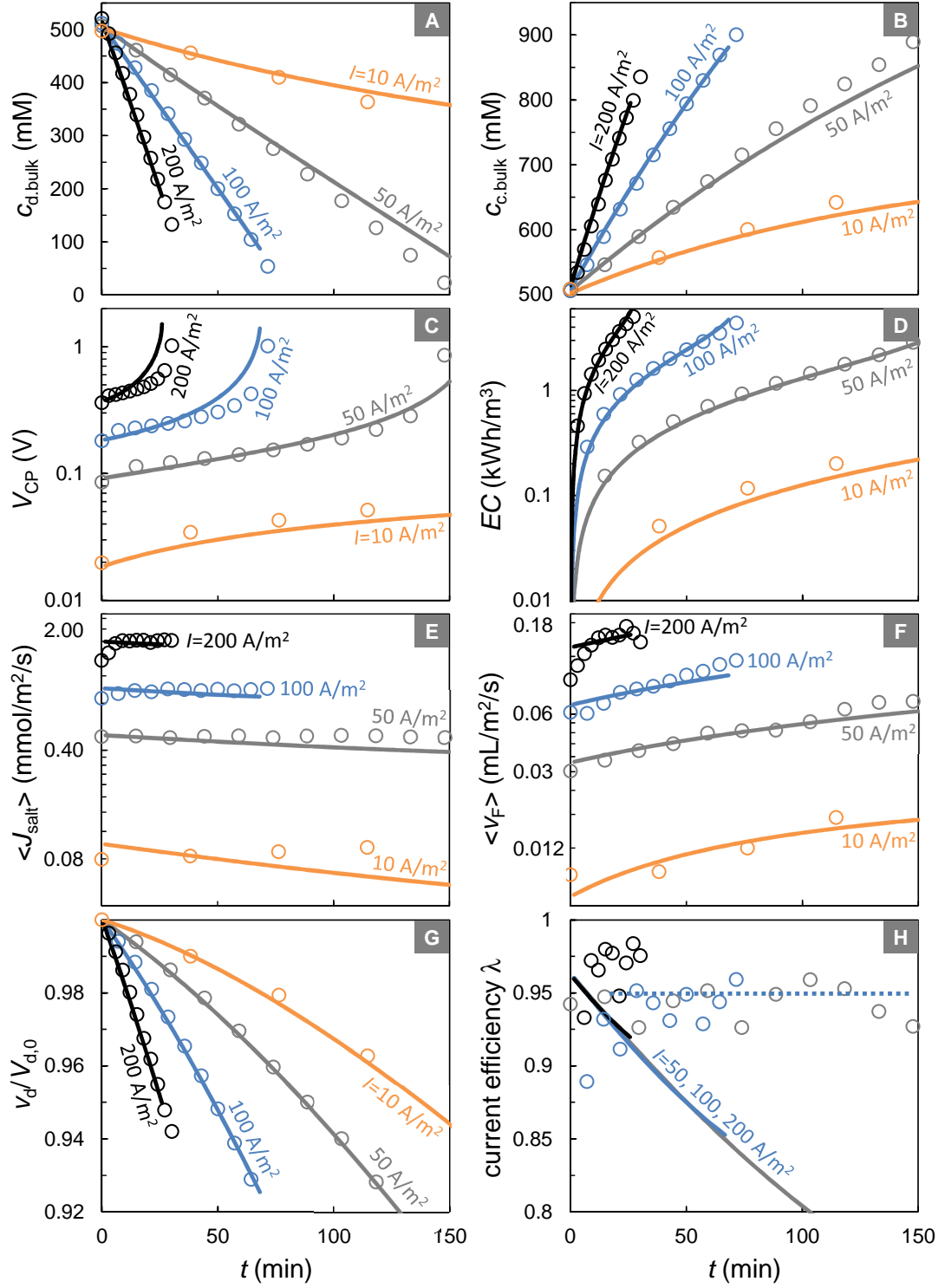


Figure 7: Performance of ED process predicted by the full model including coion and water transport (full continuous lines), compared with data (symbols) of Galama *et al.* [53] as function of time of the experiment, t . A,B) Dilute and concentrate concentration, $c_{d,bulk}$, $c_{c,bulk}$. C) Cell pair voltage, V_{CP} . D) Energy consumption, EC , in kWh per m³ of diluate. E) Average salt flux, $\langle J_{salt} \rangle$. F) Average membrane fluid velocity, $\langle v_F \rangle$. G) Normalized volume in the diluate tank, $V_d/V_{d,0}$. H) Current efficiency, λ . Dashed line refers to trendline of experimental data.

5. Conclusions

In the present work we have aimed to provide a fundamental description of transport phenomena in the (R)ED process, investigating the effect of water transport through ion-exchange membranes on process performance. In the case of negligible ion-ion friction, the Maxwell-Stefan (MS) approach we showed how the MS approach is formally equivalent to the nanofiltration theory by Deen [33]. This model extends the extended Nernst-Planck equation, which we extend in the present work with ion-ion friction. Moreover, the present model self-consistently describes fluid flow as function of the driving forces on the water, being osmotic and hydrostatic pressure gradients, and the frictions with the membrane matrix and with ions. We show how despite the extremely low water permeability of IEMs, the velocity of water in the membrane is not negligible, of the order of the velocity of the counterions.

The model shows a good agreement with two separate data sets for ED and RED, though to fit the RED-data the hydraulic permeability was possibly chosen too high. Direct ion-wall friction was (after a preliminary calculation for RED) left out from the calculation, but possibly this frictional term needs more attention. Also, the effect of the volume of the hydrated ion may have to be included in the model calculations. To further validate the model, an extended data set for the same membranes and setup, covering both ED and RED modes, is required.

Acknowledgments

This work was performed in the cooperation framework of Wetsus, European Centre of Excellence for Sustainable Water Technology (www.wetsus.eu). Wetsus is co-funded by the Dutch Ministry of Economic Affairs and Ministry of Infrastructure and Environment, the Province of Fryslân, and the Northern Netherlands Provinces. The authors thank the participants of the research theme “Blue Energy” for fruitful discussions and financial support.

References

- [1] M. Tedesco, H. V. M. Hamelers, P. M. Biesheuvel, Nernst-Planck transport theory for (reverse) electrodialysis: I. Effect of co-ion transport through the membranes, *Journal of Membrane Science* 510 (2016) 370–381.
- [2] A. A. Sonin, R. F. Probst, A hydrodynamic theory of desalination by electrodialysis, *Desalination* 5 (1968) 293–329.
- [3] T. Xu, Ion exchange membranes: State of their development and perspective, *Journal of Membrane Science* 263 (2005) 1–29.
- [4] H. J. Cassady, E. C. Cimino, M. Kumar, M. A. Hickner, Specific ion effects on the permselectivity of sulfonated poly (ether sulfone) cation exchange membranes, *Journal of Membrane Science* 508 (2016) 146–152.

- [5] C. E. Evans, R. D. Noble, S. Nazeri-Thompson, B. Nazeri, C. A. Koval, Role of conditioning on water uptake and hydraulic permeability of nafion® membranes, *Journal of Membrane Science* 279 (2006) 521–528.
- [6] M. A. Izquierdo-Gil, V. M. Barragán, J. P. G. Villaluenga, M. P. Godino, Water uptake and salt transport through Nafion cation-exchange membranes with different thicknesses, *Chemical Engineering Science* 72 (2012) 1–9.
- [7] L. Han, S. Galier, H. Roux-de Balman, Ion hydration number and electro-osmosis during electrodialysis of mixed salt solution, *Desalination* 373 (2015) 38–46.
- [8] O. Kedem, A. Katchalsky, A physical interpretation of the phenomenological coefficients of membrane permeability., *The Journal of General Physiology* 45 (1961) 143–179.
- [9] T. Holt, S. K. Ratkje, K. S. Førlund, T. Østvold, Hydrostatic pressure gradients in ion exchange membranes during mass and charge transfer, *Journal of Membrane Science* 9 (1981) 69–82.
- [10] C. Jiang, Q. Wang, Y. Li, Y. Wang, T. Xu, Water electro-transport with hydrated cations in electrodialysis, *Desalination* 365 (2015) 204–212.
- [11] P. B. Peters, R. van Roij, M. Z. Bazant, P. M. Biesheuvel, Analysis of electrolyte transport through charged nanopores, *Phys. Rev. E* 93 (2016) 053108.
- [12] Y. Tanaka, Pressure distribution, hydrodynamics, mass transport and solution leakage in an ion-exchange membrane electrodialyzer, *Journal of Membrane Science* 234 (2004) 23–39.
- [13] R. Kodým, P. Pánek, D. Šnita, D. Tvrzník, K. Bouzek, Macrohomogeneous approach to a two-dimensional mathematical model of an industrial-scale electrodialysis unit, *Journal of Applied Electrochemistry* 42 (2012) 645–666.
- [14] J. Veerman, J. W. Post, M. Saakes, S. J. Metz, G. J. Harmsen, Reducing power losses caused by ionic shortcut currents in reverse electrodialysis stacks by a validated model, *Journal of Membrane Science* 310 (2008) 418–430.
- [15] T. Teorell, Transport processes in ionic membranes, *Progress in Biophysics and Biophysical Chemistry* 3 (1953) 305–369.
- [16] R. F. Probstein, A. A. Sonin, E. Gur-Arie, A turbulent flow theory of electrodialysis, *Desalination* 11 (1972) 165–187.
- [17] R. E. Lacey, Energy by reverse electrodialysis, *Ocean Engineering* 7 (1980) 1–47.
- [18] P. N. Pintauro, D. N. Bennion, Mass transport of electrolytes in membranes. 1. Development of mathematical transport model, *Industrial and Engineering Chemistry Fundamentals* 23 (1984) 230–234.

- [19] A. G. Guzman-Garcia, P. N. Pintauro, M. W. Verbrugge, R. F. Hill, Development of a space-charge transport model for ion-exchange membranes, *AIChE Journal* 36 (1990) 1061–1074.
- [20] M. Higa, A. Tanioka, K. Miyasaka, A study of ion permeation across a charged membrane in multicomponent ion systems as a function of membrane charge density, *Journal of Membrane Science* 49 (1990) 145–169.
- [21] V. Fila, K. Bouzek, A mathematical model of multiple ion transport across an ion-selective membrane under current load conditions, *Journal of Applied Electrochemistry* 33 (2003) 675–684.
- [22] V. M. Volgin, A. D. Davydov, Ionic transport through ion-exchange and bipolar membranes, *Journal of Membrane Science* 259 (2005) 110–121.
- [23] M. Fidaleo, M. Moresi, Optimal strategy to model the electrodialytic recovery of a strong electrolyte, *Journal of Membrane Science* 260 (2005) 90–111.
- [24] J. Veerman, M. Saakes, S. J. Metz, G. J. Harmsen, Reverse electrodialysis: A validated process model for design and optimization, *Chemical Engineering Journal* 166 (2011) 256–268.
- [25] Y. Tanaka, M. Reig, S. Casas, C. Aladjem, J. L. Cortina, Computer simulation of ion-exchange membrane electrodialysis for salt concentration and reduction of RO discharged brine for salt production and marine environment conservation, *Desalination* 367 (2015) 76–89.
- [26] G. D. Mehta, T. F. Morse, E. A. Mason, M. H. Daneshpajoo, Generalized Nernst–Planck and Stefan–Maxwell equations for membrane transport, *The Journal of Chemical Physics* 64 (1976) 3917–3923.
- [27] P. Meares, Coupling of ion and water fluxes in synthetic membranes, *Journal of Membrane Science* 8 (1981) 295–307.
- [28] G. Kraaijeveld, V. Sumberova, S. Kuindersma, H. Wesselingh, Modelling electrodialysis using the Maxwell-Stefan description, *The Chemical Engineering Journal and the Biochemical Engineering Journal* 57 (1995) 163–176.
- [29] N. R. Amundson, T.-W. Pan, V. I. Paulsen, Diffusing with Stefan and Maxwell, *AIChE Journal* 49 (2003) 813–830.
- [30] C. Delacourt, J. Newman, Mathematical modeling of a cation-exchange membrane containing two cations, *Journal of the Electrochemical Society* 155 (2008) B1210–B1217.
- [31] A. H. Galama, J. W. Post, M. A. Cohen Stuart, P. M. Biesheuvel, Validity of the Boltzmann equation to describe Donnan equilibrium at the membrane-solution interface, *Journal of Membrane Science* 442 (2013) 131–139.

- [32] K. Thibault, H. Zhu, A. Szymczyk, G. Li, The averaged potential gradient approach to model the rejection of electrolyte solutions using nanofiltration: Model development and assessment for highly concentrated feed solutions, *Separation and Purification Technology* 153 (2015) 126–137.
- [33] W. M. Deen, Hindered transport of large molecules in liquid-filled pores, *AIChE Journal* 33 (1987) 1409–1425.
- [34] H. Brenner, L. J. Gaydos, The constrained brownian movement of spherical particles in cylindrical pores of comparable radius. models of the diffusive and convective transport of solute molecules in membranes and porous media, *Journal of Colloid and Interface Science* 58 (1977) 312–356.
- [35] T. R. Noordman, J. A. Wesselingh, Transport of large molecules through membranes with narrow pores: The Maxwell-Stefan description combined with hydrodynamic theory, *Journal of Membrane Science* 210 (2002) 227–243.
- [36] Y. Lanteri, P. Fievet, A. Szymczyk, Evaluation of the steric, electric, and dielectric exclusion model on the basis of salt rejection rate and membrane potential measurements, *Journal of Colloid and Interface Science* 331 (2009) 148–155.
- [37] A. Szymczyk, H. Zhu, B. Balanec, Ion rejection properties of nanopores with bipolar fixed charge distributions, *The Journal of Physical Chemistry B* 114 (2010) 10143–10150.
- [38] P. M. Biesheuvel, Two-fluid model for the simultaneous flow of colloids and fluids in porous media., *Journal of Colloid and Interface Science* 355 (2011) 389–95.
- [39] A. E. Yaroshchuk, Transport properties of long straight nano-channels in electrolyte solutions: A systematic approach, *Advances in Colloid and Interface Science* 168 (2011) 278–291.
- [40] A. A. Sonin in: E. Sélégny, *Charged Gels and Membranes I*, D. Reidel Publishing Company, 1976.
- [41] E. Spruijt, P. M. Biesheuvel, Sedimentation dynamics and equilibrium profiles in multicomponent mixtures of colloidal particles, *Journal of Physics: Condensed Matter* 26 (2014) 075101.
- [42] R. Schlögl, *Stofftransport durch Membranen*, Dr. Dietrich Steinkopff Verlag.
- [43] F. G. Helfferich, *Ion Exchange*, Mc Graw-Hill, London, 1962.
- [44] K. Kontturi, L. Murtomäki, J. A. Manzanares, *Ionic Transport Processes: In Electrochemistry and Membrane Science*, OUP Oxford, 2008.
- [45] J. Veerman, R. M. de Jong, M. Saakes, S. J. Metz, G. J. Harmsen, Reverse electrodialysis: Comparison of six commercial membrane pairs on the thermodynamic efficiency and power density, *Journal of Membrane Science* 343 (2009) 7–15.

- [46] E. Güler, R. Elizen, D. A. Vermaas, M. Saakes, K. Nijmeijer, Performance-determining membrane properties in reverse electrodialysis, *Journal of membrane Science* 446 (2013) 266–276.
- [47] J. Catalano, H. V. M. Hamelers, A. Bentien, P. M. Biesheuvel, Revisiting morrison and osterle 1965: the efficiency of membrane-based electrokinetic energy conversion, *Journal of Physics: Condensed Matter* 28 (2016) 324001.
- [48] C.-O. Danielsson, A. Dahlkild, A. Velin, M. Behm, A model for the enhanced water dissociation on monopolar membranes, *Electrochimica Acta* 54 (11) (2009) 2983 – 2991.
- [49] H. Strathmann, Ion-exchange membrane separation processes, Vol. 9, Elsevier Science Limited, 2004.
- [50] M. Tedesco, C. Scalici, D. Vaccari, A. Cipollina, A. Tamburini, G. Micale, Performance of the first Reverse Electrodialysis pilot plant for power production from saline waters and concentrated brines, *Journal of Membrane Science* 500 (2016) 33–45.
- [51] R. S. Kingsbury, K. Chu, O. Coronell, Energy storage by reversible electrodialysis: The concentration battery, *Journal of Membrane Science* 495 (2015) 502–516.
- [52] J. W. van Egmond, M. Saakes, S. Porada, T. Meuwissen, C. J. N. Buisman, H. V. M. Hamelers, The concentration gradient flow battery as electricity storage system: Technology potential and energy dissipation, *Journal of Power Sources* 325 (2016) 129–139.
- [53] A. H. Galama, M. Saakes, H. Bruning, H. H. M. Rijnaarts, J. W. Post, Seawater predesalination with electrodialysis, *Desalination* 342 (2014) 61–69.